Mechanism for SO2 poisoning of Cu-CHA during low temperature NH3-SCR

Citation for the original published paper (version of record):
Bjerregaard, J., Votsmeier, M., Grönbeck, H. (2023). Mechanism for SO2 poisoning of Cu-CHA during low temperature NH3-SCR. Journal of Catalysis, 417: 497-506.
http://dx.doi.org/10.1016/j.jcat.2022.12.023

Journal of Catalysis 417 (2023) 497–506

Contents lists available at ScienceDirect

Journal of Catalysis

journal homepage: www.elsevier.com/locate/jcat

Mechanism for SO_2 poisoning of Cu-CHA during low temperature NH_3-SCR

Joachim D. Bjerregaard [a,*], Martin Votsmeier [b], Henrik Grönbeck [a,*]

[a] Department of Physics and Competence Centre for Catalysis, Chalmers University of Technology, SE-412 96 Göteborg, Sweden
[b] Umicore AG & Co. KG, Rodenbacher Chaussee 4, 63457 Hanau, Germany

ARTICLE INFO

Article history:
Received 7 October 2022
Revised 2 December 2022
Accepted 19 December 2022
Available online 24 December 2022

Keywords:
SO_2 poisoning
Cu-CHA
NH_3-SCR
Ammonium bisulfate
Diffusion

ABSTRACT

Density Functional Theory (DFT) calculations are used to investigate low temperature SO_2 deactivation of Cu-CHA during ammonia assisted selective catalytic reduction of NO (NH_3-SCR). SO_2 is found to adsorb on $[Cu^{II}_2(NH_3)_4O_2]^{2+}$ forming a copper sulfate complex. NO and NH_3 react over the sulfate complex forming N_2, H_2O and H_2SO_4. H_2SO_4 undergoes an acid-base reaction with NH_3 yielding $SO_4(NH_4)_2$ and $HSO_4(NH_4)$, where $HSO_4(NH_4)$ is thermodynamically preferred during typical reaction conditions. The SO_2-derived species are bulky and have considerable barriers for inter-cage diffusion. Moreover, the presence of $HSO_4(NH_4)$ species reduces the probability of having two $[Cu^{I}(NH_3)_2]^{+}$ complexes in one cage, which is a requirement for O_2 activation. The results suggest that the key mechanism for low temperature SO_2 deactivation is of physical origin and that the catalyst can be regenerated by exposure to high temperatures where $HSO_4(NH_4)$ decomposes. The suggested mechanism agrees with experimental observations and provides atomistic understanding of sulfur poisoning of Cu-CHA during NH_3-SCR.

1. Introduction

Exhaust from combustion engines contains hazardous nitrogen oxides (NO_x), which should be removed by an aftertreatment system [1]. NO_x in oxygen excess can efficiently be reduced to N_2 and H_2O via ammonia assisted selective catalytic reduction (NH_3-SCR) over transition metal functionalized small pore zeolites. In particular, copper exchanged chabazite (Cu-CHA) has shown good low-temperature catalytic activity and selectivity [2,3] and simultaneously a good hydrothermal stability [4,5]. The overall reaction scheme for the, so called, standard NH_3-SCR reaction is

$$4NH_3 + 4NO + O_2 \rightarrow 4N_2 + 6H_2O \quad \text{(R1)}$$

The NH_3 to NO ratio is one and O_2 is required for the hydrogen abstraction. The catalytic reaction is a redox cycle, where the oxidation state of Cu changes between Cu^{I} and Cu^{II}. Cu^{I} is oxidized to Cu^{II} upon O_2 adsorption and reduced to Cu^{I} during NH_3-NO coupling. The catalytic activity has been measured to have a quadratic dependence on the copper loading at low temperatures, which suggests that two copper ions are involved in the standard SCR mechanism [6–8]. Thus, the diffusion and paring of the copper ions is a critical step for the low-temperature activity. Two experimentally reported states of the Cu-ions are Z_2Cu and ZCuOH [9,10]. Z refers to the Al-environment; Z being one Al-site and Z_2 two Al-sites. The copper ions are solvated in the presence of ammonia, forming mobile $[Cu^{I}(NH_3)_2]^{+}$ complexes [11–14], which diffuse between the zeolite cages with small barriers [15,16]. By having two $[Cu^{I}(NH_3)_2]^{+}$ complexes in the same cage, O_2 can be activated forming a $[Cu^{II}_2(NH_3)_4O_2]^{2+}$ peroxo complex, over which NO and NH_3 couple to H_2NNO and HONO. It has been suggested that H_2NNO and HONO decompose to N_2 and H_2O over Brønsted acid sites [17,18].

Despite high activity and selectivity, one issue with the Cu-CHA catalyst is a sensitivity to SO_2 and SO_3 exposure. Even small concentrations of sulfur compounds in the exhaust have shown to accumulate in the catalyst and significantly decrease the SCR-activity [19–21], which lowers the operational lifetime of the catalyst. The mechanism behind the deactivation is not well understood and the degree of deactivation appears to depend on numerous variables such as temperature, gas composition, Cu loading, Si/Al ratio and the state of the Cu-ion (ZCuOH or Z_2Cu) [19,22,23]. Moreover, SO_2 and SO_3 shows differences in the degree of induced deactivation, with SO_3 being more severe [24]. Presence of SO_3 in the exhaust stream could originate from the diesel oxidation catalyst (DOC) commonly placed upstream of the NH_3-SCR catalyst.

* Corresponding authors.
E-mail addresses: joabje@chalmers.se (J.D. Bjerregaard), ghj@chalmers.se (H. Grönbeck).

https://doi.org/10.1016/j.jcat.2022.12.023
0021-9517/

The SO_2-deactivation can be divided into reversible and irreversible deactivation [25,20]. The deactivation for Cu-CHA is predominately reversible and the catalyst activity can be regained by periodically heating to 500–550 °C [20,26]. The reversible deactivation has been measured to be pronounced over a wide range of S/Cu ratios and associated with a lowering of the apparent activation energy of the SCR reaction [25]. The reversible deactivation can, therefore, not be directly related to sulfur adsorption at copper sites. Recent measurements have instead indicated that SO_2 affect the mobility and redox behavior of copper species [27]. The irreversible deactivation has been measured to have a close to 1:1 relationship between the deactivation and the S/Cu ratio. Furthermore, the apparent activation energy of the SCR reaction does not change dramatically during the irreversible deactivation [25]. This suggests that the irreversible deactivation is related to sulfur species that blocks the copper sites.

The interaction of SO_2 with copper species and reaction intermediates during low temperature NH_3-SCR is not well understood. Using X-ray absorption spectroscopy measurements, Molokova et al., [28] studied recently the reactivity of SO_2 with different reaction intermediates. It was found that SO_2 is reactive towards the peroxo species $[Cu^{II}_2(NH_3)_4O_2]^{2+}$ reducing the Cu-ion from Cu^{II} to Cu^{I}. Although first-principles calculations have been used to investigate mechanisms for the NH_3-SCR reaction in Cu-CHA [17,18,29,30,7], the influence of sulfur on the reaction has mainly concerned the relative thermodynamic stability [31,22] of different sulfur containing species and the reaction of SO_x with framework bound copper, namely Z_2Cu and ZCuOH [23,32]. The conclusions from the thermodynamic analyses are that copper bisulfates ($CuHSO_4$) and copper ammonium sulfate ($CuSO_4(NH_4)$) are the preferred species during reaction conditions [31,22]. A higher stability has been predicted for SO_x species formed over ZCuOH as compared to Z_2Cu. In addition, SO_3 adsorption over ZCuOH has been found to form $CuHSO_x$ complexes with higher stability than adsorption of SO_2 over ZCuOH [23,32].

Herein, we use DFT calculations to study the mechanism for low temperature SO_2 deactivation of Cu-CHA during NH_3-SCR. Reaction landscapes, diffusion paths, and thermodynamic preferences are investigated. We find that SO_2 interacts strongly with the peroxo complex $[Cu^{II}_2(NH_3)_4O_2]^{2+}$, forming primarily ammonium bisulfate ($HSO_4(NH_4)$) under reaction conditions. The sulfur species are found to accumulate in the CHA cage due to high diffusion barriers. The presence of sulfate species in the cage reduces the stability of paired $[Cu^{I}(NH_3)_2]^{+}$ complexes, which are required for O_2 activation, thereby deactivating the catalyst. Our work provides insights and possible explanations for the considerable deactivation by small amounts of SO_2 in Cu-CHA and highlights the importance of facile $[Cu^{I}(NH_3)_2]^{+}$ diffusion and pairing for maintained NH_3-SCR activity.

2. Computational methods

2.1. DFT calculations

Spin polarised density functional theory (DFT) calculations are performed with the Vienna Ab initio Simulation Package (VASP) [33,34]. The Perdew-Burke-Ernzerhof (PBE) [35] version of the generalized gradient approximation is used to describe the exchange–correlation energy. The Grimme D3 approach [36] is applied to account for van der Waals interactions and a Hubbard term of 6 eV [37] is employed to reduce spurious delocalization of the Cu 3d electrons. The combination of Grimme D3 and PBE + U(6) has previously been shown to describe the Cu-CHA with reasonable accuracy when compared to experimental temperature programmed desorption (TPD) measurements of NH_3, stability of Cu_2O_2-motif crystals and XPS/UPS spectra of copper oxides [38]. Pure GGA functionals tend to overestimate the binding energy for adsorption of NO on copper, when compared to hybrid functionals [39] and the inclusion of the Hubbard-U term is crucial to describe the changes in the oxidation states of Cu [38].

The Kohn–Sham orbitals are expanded with plane waves using a cut-off value of 480 eV and the interaction between the valence electrons and core is described by the Projector Augmented Wave (PAW) method [40,41]. The valence electrons considered for each element is Cu(11), Si(4), S(6), Al(3), O(6), N(5), and H(1). The k-point sampling is restricted to the gamma point. The self-consistent field (SCF) loop is considered to be converged, when the energy difference is less than 10^{-5} eV, and the structure is considered to be a minimum if the norm of all forces acting on the atoms is lower than 0.02 eV/Å The transition states are determined by the climbing image nudged elastic band (CI-NEB) method [42,43], and confirmed by vibrational analysis showing only one imaginary frequency. The vibrational analysis is done using the method of finite differences. All reaction landscapes are zero-point corrected. To explore the flat energy landscape for the different species in the zeolite, ab initio molecular dynamics (AIMD) simulations are performed and structures are relaxed from several point along the AIMD trajectory. The temperature is in the AIMD controlled using a Nosé-Hoover thermostat in the NVT ensemble [44,45]. The mass of hydrogen is replaced with that of tritium to facilitate integration of the equations of motion allowing a time step of 1 fs. In addition, constrained AIMD simulations are performed to explore both the inter- and intra-cage diffusion of various species. The free energy change along the trajectory is evaluated by thermodynamic integration of the free energy gradients [46]. Bader charge analyses are performed as implemented by the Henkelman group [47,48]. The CHA cage is modelled with a hexagonal unit cell consisting of 34 Si, 2 Al, and 72 O atoms, corresponding to a Si/Al ratio of 17, which is within the range of typical experimental values [22,23,20]. When two copper species are placed inside the cage, two aluminum atoms are placed opposite to each other in one six-membered ring, which previously has been reported to represent a stable configuration [49]. The choice of the Al configuration could potentially influence the energetics of the system. It has been shown that the stability of activated O_2 on paired $[Cu^{I}(NH_3)_2]^{+}$ complexes can change up to 0.2 eV for relevant Al configurations [50]. However, the energy involved in SO_2 adsorption, is significantly higher than 0.2 eV, suggesting that the choice of Al configuration will not affect the main conclusions in the present study.

2.2. Construction of phase diagrams

To evaluate the relative stability of different species as a function of temperature and NH_3 pressure, we construct phase diagrams from the relative Gibbs free energies of formation.

$$Z_2Cu_2 + \left(\frac{a}{2} - c - \frac{d-3b}{4}\right)\cdot O_2 + b\cdot NH_3 + \left(\frac{d-3b}{2}\right)\cdot H_2O + c \cdot SO_2 \longrightarrow Z_2Cu_2S_cO_aN_bH_d \quad (1)$$

The considered reservoirs are the gas phase species SO_2, H_2O, O_2, NH_3 and the framework bound copper Z_2Cu_2. The Gibbs free energy of formation is calculated for each state according to:

$$\Delta G = E^{DFT} - c\cdot\Delta\mu_{SO_2} - \left(\frac{a}{2} - c - \frac{d-3b}{4}\right)\cdot\Delta\mu_{O2} - \left(\frac{d-3b}{2}\right)\cdot\Delta\mu_{H_2O} - b\cdot\Delta\mu_{NH_3} - T\Delta S(T) \quad (2)$$

We neglect the pV term and approximate the enthalpy as the zero-point corrected electronic energy (E^{DFT}). E^{DFT} is given by

$$E^{DFT} = E^{DFT}_{Z_2Cu_2S_cO_aN_bH_d} - E^{DFT}_{Z_2Cu_2} - \left(\frac{a}{2} - c - \frac{d-3b}{4}\right)\cdot E^{DFT}_{O_2} - b\cdot E^{DFT}_{NH_3} - \left(\frac{d-3b}{2}\right)\cdot E^{DFT}_{H_2O} - c\cdot E^{DFT}_{SO_2} \quad (3)$$

By including the chemical potential ($\Delta\mu_x$), the stability as a function of SO_2, H_2O, NH_3 and O_2 pressure is taken into account.

$$\mu_x(p_x,T) = k_b\cdot T\cdot \ln\left(\frac{p_x}{p^o}\right) - T\Delta S(T)_x \quad (4)$$

The entropies of the gas phase species are taken from the JANAF table [51], and is linearly interpolated between the experimental data points. Estimation of the adsorbate entropies inside the zeolite cages are challenging as it may contain a significant amount of translational and rotational entropy, which are not captured properly in the harmonic approximation [10,17,52]. However, in this study we have considered bulky SO_4^{2-}, $[Cu^I(NH_3)_2]^+$ and NH_4^+ species confined in the small CHA cage, which implies that the translation and rotational degrees of freedom are significantly reduced. We have, therefore, assumed that the adsorbates lose most of their rotational and translational entropy and have evaluated these contributions as frustrated vibrations.

3. Results

3.1. Reaction cycle with SO_2

Copper is solvated by two ammonia ligands forming $[Cu^I(NH_3)_2]^+$ during typical reaction conditions[11–14]. Previously proposed reaction cycles have shown that a key step for the NH_3-SCR reaction is the adsorption of O_2 on a pair of $[Cu^I(NH_3)_2]^+$ forming a peroxo complex $[Cu^{II}_2(NH_3)_4O_2]^{2+}$[7,17,18,53]. NO and NH_3 can couple over the peroxo complex forming H_2NNO and HONO, which can diffuse to Brønsted acid site and decompose to H_2O and N_2[17,18].

The proposed reaction cycles for NH_3-SCR [17,18] are here extended by the interaction with SO_2 (Fig. 1). The reaction consists of one cycle without chemical bonds to the framework (the outer circle with structures denoted by roman numbers). However, a part of the reaction is able to follow an alternative route, forming chemical bonds to the framework (the inner circle with structures denoted by letters). The corresponding energy landscapes are

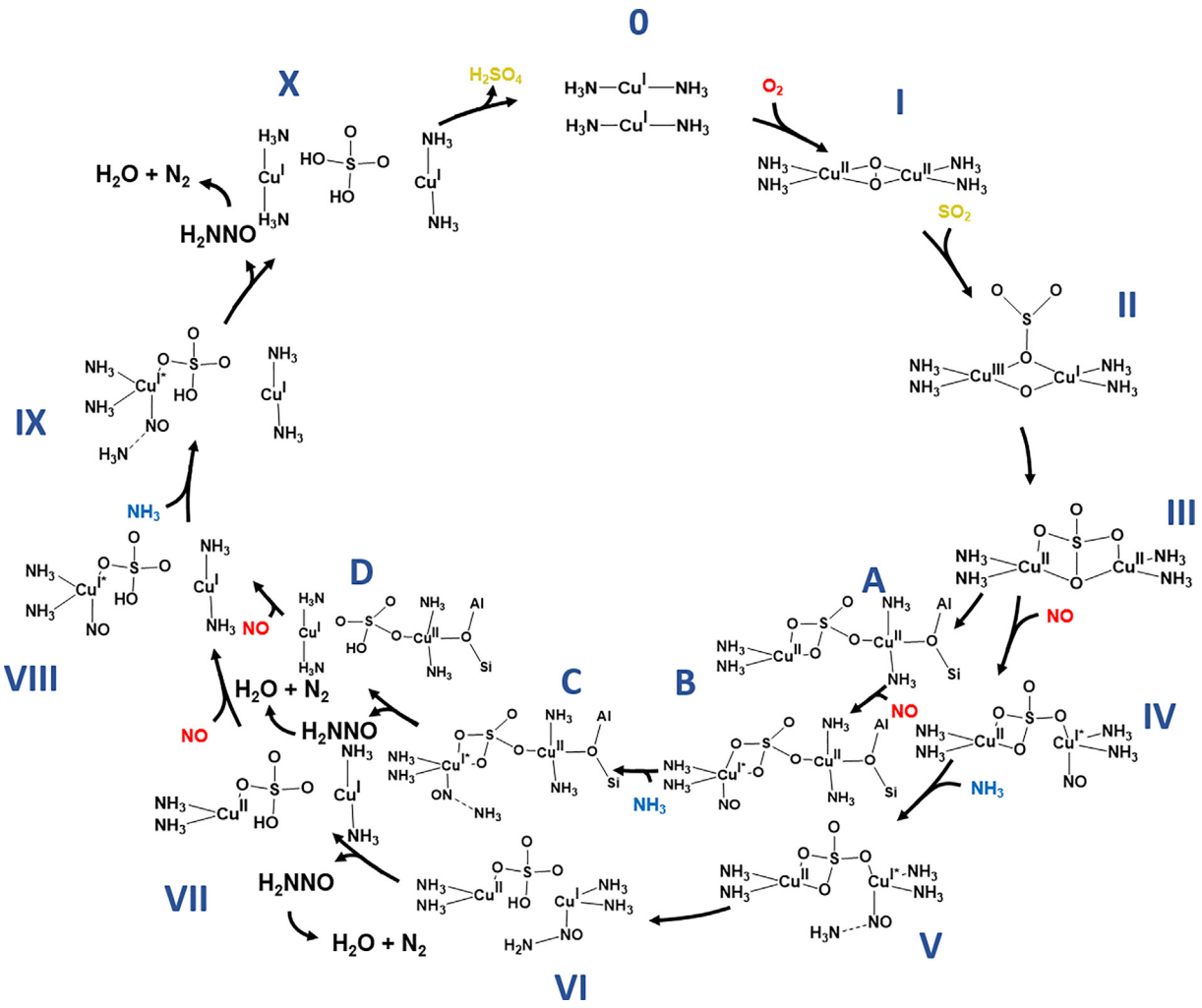

Fig. 1. Proposed reaction cycle for low temperature NH_3-SCR in the presence of SO_2. The oxidation state for Cu is indicated. Al-O-Si represents a Brønsted acid site, and is only shown if the $[Cu^I(NH_3)_2]^+$ complex is chemically bound to the framework. Oxidation state of I* indicate an intermediate oxidation state between I and II with magnetic moment of 0.2–0.3. H_2SO_4 is formed during the SCR reaction.

reported in Figs. 2 and 3. Note that the energy landscapes include more structures than the catalytic cycles.

The starting point of the considered reaction is two $[Cu^{I}(NH_3)_2]^+$ complexes in the same CHA-cage (structure **0**). One suggestion for the origin of this configuration could be the reduction of a Z_2Cu site, initially forming $[Cu^{I}(NH_3)_2]^+$ and a Brønsted acid site, that in presence of NH_3, would be NH_4^+. As $[Cu^{I}(NH_3)_2]^+$ and NH_4^+ are mobile, the NH_4^+ ion could diffuse to a neighboring cage, and a second $[Cu^{I}(NH_3)_2]^+$ complex could counter diffuse into the cage to retain the charge neutrality. This type of exchange is also the basis of the solid-state ion exchange [15].

We find that SO_2 interacts weakly with $[Cu^{I}(NH_3)_2]^+$ (structure **0**) without any chemical bonds. SO_2 is merely coordinated to the Cu^+ ion with a long (O-Cu) distance of 3.0 Å. SO_2 interacts instead strongly with the peroxo complex (**I** ⇒ **II**). In this case, SO_2 adsorbs on one oxygen atom with an adsorption energy of −0.51 eV, forming SO_3 with an S-O bond length of 1.6 Å One of the copper ions is oxidized to Cu^{III} upon formation of SO_3. From a Bader analysis, we find that sulfur in SO_3 is close to a +4 oxidation state, similar to the case of SO_2. The SO_3 species reacts without barrier with the second oxygen forming a very stable sulfate species (**III**). The sulfate species is preferred by 2.59 eV with respect to structure **II**. The oxidation state of sulfur is +6 in structure **III**. The formation of sulfur in a +6 oxidation state upon SO_2 exposure of Cu-CHA has previously been observed using XAS and XPS [22,54,55]. The two copper ions in **III** are in +2 oxidation states (Cu^{II}), thus providing the two electrons needed to form a sulfate (SO_4^{2-}). NH_3 and NO can react over **III** in a similar fashion as in the previously proposed low temperature NH_3-SCR cycles [17,18]. NO adsorbs at the Cu-site with a bond length of 2.04 Å and an adsorption energy of −0.91 eV giving structure **IV**. NO adsorption results in the breaking of one of the Cu–O bonds. An electron is transferred during the adsorption forming NO^+ and a partially reduced Cu. Attempts to adsorb NO at an oxygen anion did not result in any chemical bond. As NO is positively charged, NH_3 can coordinate to NO, with an N-N length of 2.03 Å and an adsorption energy of −0.30 eV (Structure **V**). One of the hydrogen atoms in H_3NNO-Cu is only 2.10 Å from the nearest oxygen and transfers without barrier to the oxygen forming H_2NNO and a copper bisulfate (**V** ⇒ **VI**).

As the bisulfate species (HSO_4^-) only is singly charged, one of the Cu ions is reduced (Cu^{II} ⇒ Cu^{I}), which is accompanied by the breaking of one of the Cu–O bonds. The H_2NNO group can desorb, diffuse and decompose over a Brønsted acid site (**VI** ⇒ **VII**) forming N_2 and H_2O [17]. The adsorption of NO and NH_3, can be repeated on structure **VII** where NO is adsorbed on the Cu^{II} site bound to the bisulfate. This proceeds with an adsorption energy of −0.93 eV and −0.61 eV for NO (structure **VIII**) and NH_3 (structure **IX**), respectively. The hydrogen transfer has a low barrier of 0.28 eV, which breaks the O-Cu bond and results in two $[Cu^{I}(NH_3)_2]^+$ species and one sulfuric acid molecule.

An alternative reaction path where copper binds to the framework is described in the inner circle of Fig. 1, with the reaction landscape reported in Fig. 3. Structure **III** can be turned into a framework bound species (structure **A**) via barriers of 0.28 eV and 0.09 eV. In structure **A** of Fig. 3, Cu binds to a Brønsted acid site forming a square planar-like species. Structure **III′** is separated by a barrier of only 0.09 eV to structure **A**, which is energetically preferred by −0.6 eV with respect to the mobile complex. NO and NH_3 can react over structure **A** in a similar fashion as discussed for the mobile complexes. The adsorption energies of NO and NH_3 are −0.25 eV (structure **B**) and −0.57 eV (structure **C**), respectively. The hydrogen transfer has a barrier of 0.09 eV forming bisulfate (structure **C′**). As already discussed, the H_2NNO group can desorb and decompose into H_2O and N_2. The adsorption of the second NO in the reaction cycle, which is done on the framework bound Cu, results in a partially reduction of the Cu ion. The reduction leads to the breaking of the Al-O-Cu bond, forming structure **VIII**. From here on, the reaction proceeds along the outer circle in Fig. 1.

Closing the catalytic cycle requires that H_2SO_4 leaves the cage. Our calculations show that the barrier for H_2SO_4 diffusion to a neighboring cage is 1.45 eV, see Fig. 4, which indicates that H_2SO_4 at low temperatures will accumulate in the CHA-cage.

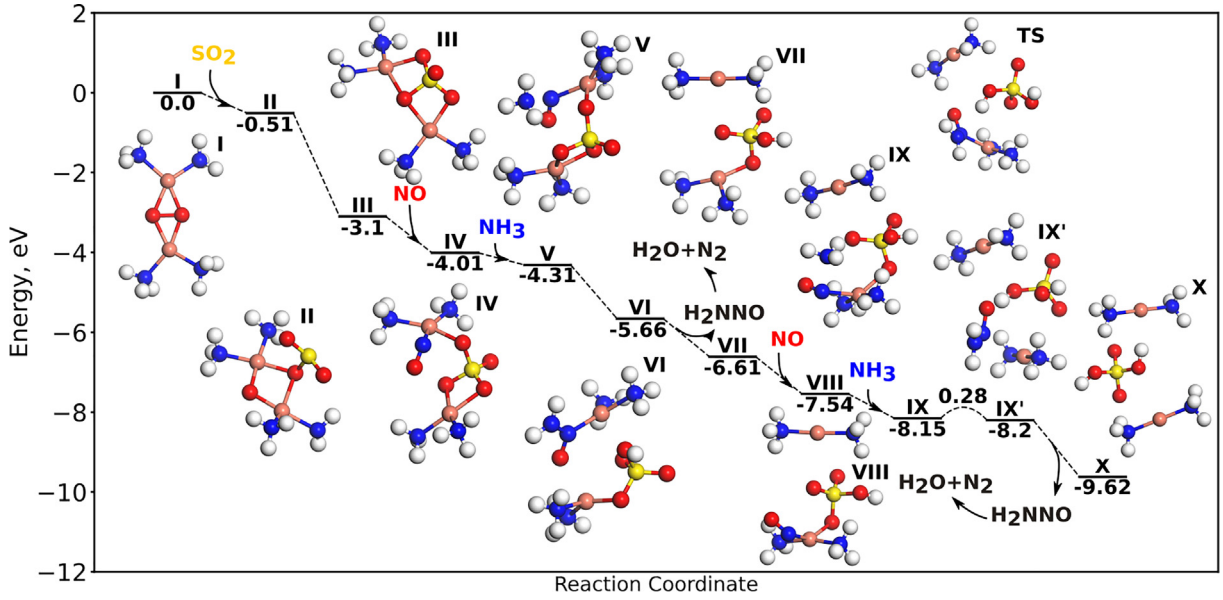

Fig. 2. Energy landscape for the proposed reaction cycle for low temperature NH_3-SCR in the presence of SO_2 without any framework bound $[Cu^{I}(NH_3)_2]^+$. (Outer circle in Fig. 1.) The zeolite cage is not shown for clarity. Atomic color codes: H(white), N(blue), O(red), S(yellow). and Cu(Bronze). (For interpretation of the references to colour in this figure legend, the reader is referred to the web version of this article.)

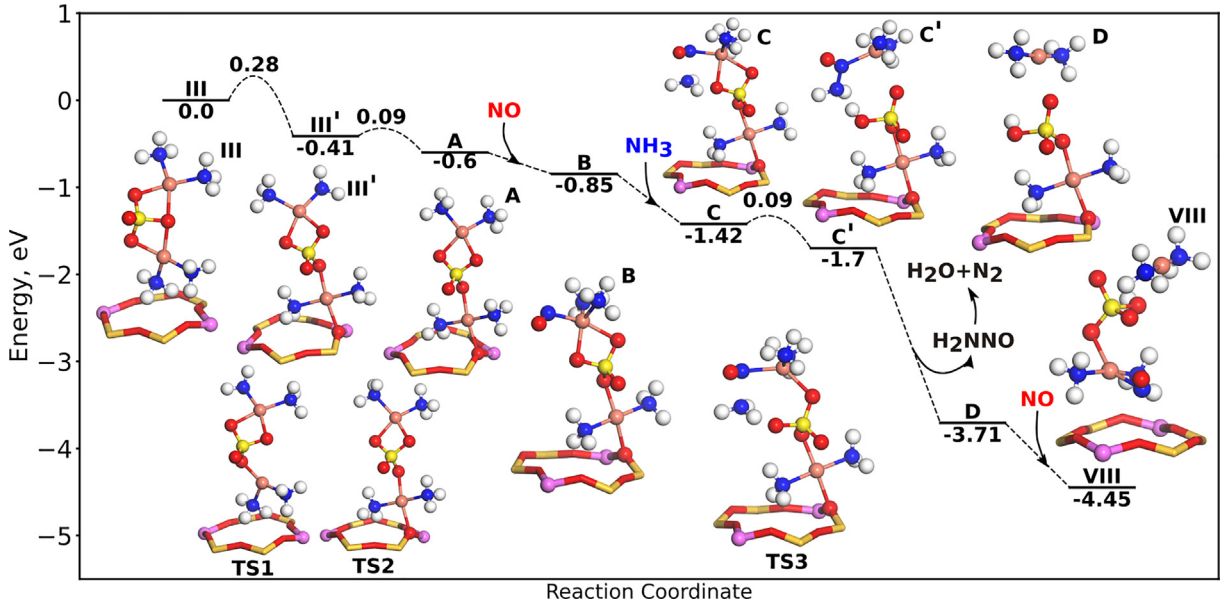

Fig. 3. Energy landscape for the proposed reaction cycle for low temperature NH_3-SCR with framework bound $[Cu^{I}(NH_3)_2]^+$. (Inner circle in Fig. 1.) Only the six-membered ring of CHA is shown. Atomic color codes as in Fig. 2 with Si(dark yellow sticks) and Al(pink). (For interpretation of the references to colour in this figure legend, the reader is referred to the web version of this article.)

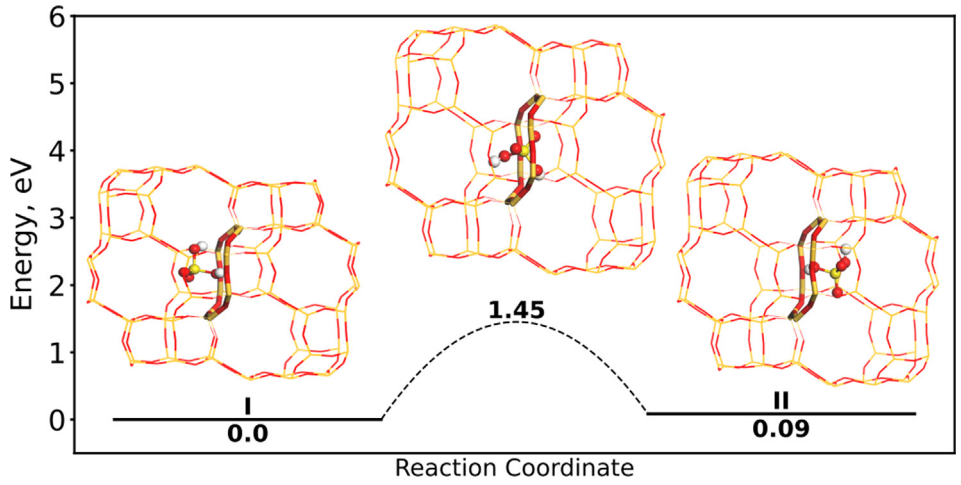

Fig. 4. Energy landscape for diffusion of H_2SO_4, through an eight-membered ring in CHA. Atomic color codes as in Fig. 3.

3.2. Formation of ammonium (bi) sulfate

Sulfuric acid (H_2SO_4) is one of the products in the reaction cycle described in Fig. 1. However, sulfuric acid can in the presence of NH_3 undergo an acid-base reaction forming ammonium bisulfate ($HSO_4(NH_4)$) and ammonium sulfate ($SO_4(NH_4)_2$), (**R2** and **R3**).

$$H_2SO_4 + NH_3 \rightleftharpoons HSO_4(NH_4) \quad (R2)$$

$$HSO_4(NH_4) + NH_3 \rightleftharpoons SO_4(NH_4)_2 \quad (R3)$$

AIMD simulations at 473 K reveal that the protons bonded to SO_4 are exchanged spontaneously forming either $HSO_4(NH_4)$ or $SO_4(NH_4)_2$, if an NH_3 molecule is added to the CHA-cage. Thus, the simulations suggest that the activation barriers to form $HSO_4(NH_4)$ and $SO_4(NH_4)_2$ are negligible. To investigate the dominant species at NH_3-SCR conditions, a phase diagram assessing the thermodynamic stability as a function of temperature and ammonia pressure is presented in Fig. 5. The structures considered in the phase diagram are two $[Cu^{I}(NH_3)_2]^+$ complexes together with H_2SO_4, $HSO_4(NH_4)$, and $SO_4(NH_4)_2$. This represents the state of the catalyst after H_2SO_4 is formed corresponding to structure **X** in Fig. 1. The gas-phase concentrations used to construct the phase diagram are 10 % O_2, 5 % H_2O and 20 ppm SO_2. The arrow represents a typical ammonia concentration under SCR conditions (p_{NH3} = 300 ppm). At reaction conditions (T = 200 °C), it is clear that the dominant species is $HSO_4(NH_4)$, whereas $SO_4(NH_4)_2$ requires higher pressures of NH_3 or lower temperatures. H_2SO_4 is not stable enough to be present in the phase diagram. Thus, as soon as H_2SO_4 is formed in presence of NH_3 it will react to $HSO_4(NH_4)$. Note that $HSO_4(NH_4)$ and the mobile $[Cu^{I}(NH_3)_2]^+$ complexes are predicted to decompose simultaneously, which is a consequence of their mutual stabilization. We stress that the phase diagram only represents the equilibrium situation without possible kinetic limitations and the assumption that the concentration of ammonia is the same in the gas phase as inside the CHA cage.

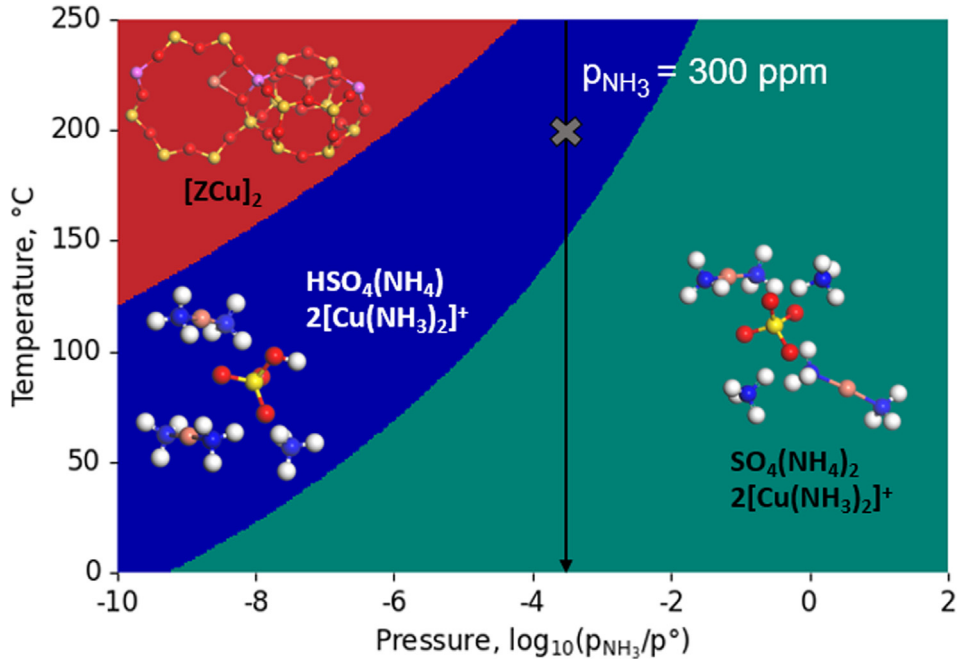

Fig. 5. Phase diagram showing the state of Cu and sulfur-containing species. Structures considered in the phase diagram are framework $[ZCu]_2$, H_2SO_4, $HSO_4(NH_4)$ and $SO_4(NH_4)_2$. The pressures for the gas phase species are set to 10 % for O_2, 5 % for H_2O, and 20 ppm for SO_2. The black arrow represents an NH_3 pressure of 300 ppm. The grey cross indicates typical reaction conditions of 300 ppm NH_3 and 200 °C. Atomic color codes as in Fig. 3.

The phase diagram is constructed with acid-base reactions with structure **X** in Fig. 1. Exchange of protons between NH_3 and sulfur-species could also take place early in the reaction cycle. One possibility is NH_3 reacting with copper bisulfate, structure **VII** in Fig. 1. Structure **VII**, will form copper ammonium bisulfate in presence of NH_3 (**R4**).

$$(NH_3)_2CuSO_4H + NH_3 \rightleftharpoons (NH_3)_2CuSO_4(NH_4) \quad (R4)$$

This reaction is barrierless and exothermic, see Supplementary Material (SM).

3.3. Possible deactivation routes

The catalytic cycle (Fig. 1) and the phase diagram (Fig. 5) indicate that sulfate species will accumulate in CHA cages during reaction conditions, however the results do not reveal why and how the accumulation leads to deactivation. An important step in low temperature NH_3-SCR is the activation of O_2 by a pair of $[Cu^{I}(NH_3)_2]^{+}$ complexes, forming a peroxo complex ($[Cu^{II}_2(NH_3)_4O_2]^{2+}$). Here we investigate how the formation of the peroxo complex is affected by the presence of a bisulfate species. The potential energy diagram for O_2 activation in presence of ammonium bisulfate is shown in Fig. 6. Structure **I**, represents the catalytic site after the reaction cycle in Fig. 1, thus H_2SO_4 and two $[Cu^{I}(NH_3)_2]^{+}$ complexes. The first step, (**I** ⇒ **II**), is intra cage diffusion of the two $[Cu^{I}(NH_3)_2]^{+}$ complexes to be close enough for O_2 adsorption. The diffusion is barrierless according to constrained AIMD simulations (see SM). The adsorption energy for oxygen is 0.08 eV (structure **III**). The adsorption energy is 0.2 eV

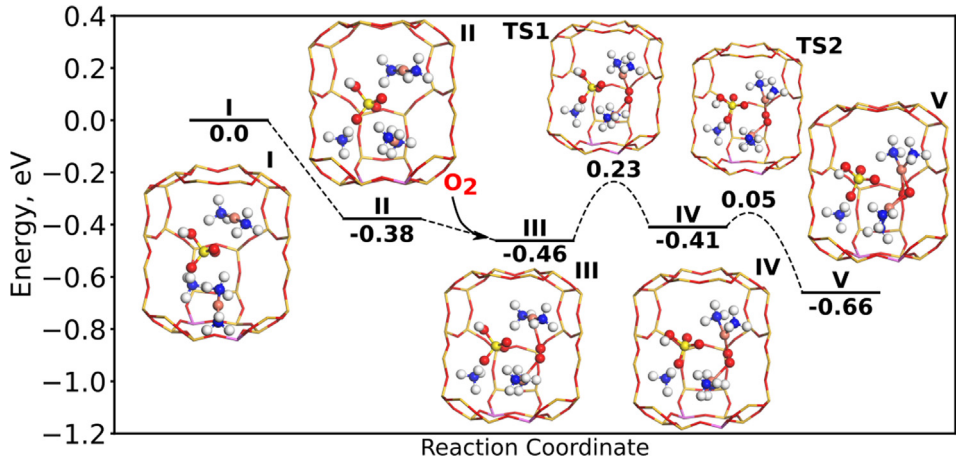

Fig. 6. Energy landscape for the formation of $[Cu^{II}(NH_3)_4O_2]^{2+}$ in the presence of $HSO_4(NH_4)$ in the zeolite cage. Atomic color codes as in Fig. 3.

in the absence of ammonium bisulfate,[17] thus the presence of ammonium bisulfate lowers the adsorption energy. We note that the O_2 adsorption energy is likely underestimated using the applied computational approach,[18] and that the reduction of the adsorption energy in the presence of ammonium bisulfate has a higher significance than the absolute energy. Although a reduced O_2 adsorption energy slows down the reaction, the reaction may still proceed and the mere presence of ammonium bisulfate is likely not the cause of deactivation.

The subsequent barriers to form the peroxo complex (structure **V**) are 0.23 eV and 0.05 eV, respectively. The formed peroxo complex has a bent configuration and similar structures are obtained also in the presence of H_2SO_4 and $SO_4(NH_4)_2$ (see SM). NO can adsorb on the bent peroxo species forming NO^+, which is required for the coupling of NO and NH_3 and the formation of H_2NNO[18]. Thus, the NH_3-SCR appears to proceed also in the presence of one $HSO_4(NH_4)$. Similar results are calculated for O_2 adsorption in the presence of H_2SO_4 and $SO_4(NH_4)_2$, see SM. O_2 is found to adsorb on a $[Cu^I(NH_3)_2]^+$ pair also in the presence of two $HSO_4(NH_4)$ in the cage forming a third $HSO_4(NH_4)$ with a reaction landscapes similar to that in Fig. 6.

To evaluate the thermodynamic stability of multiple $SO_4(NH_4)_2$ species, a phase diagram is constructed. The phase diagram contains zero, one, two and three $HSO_4(NH_4)$ species together with the two $[Cu^I(NH_3)_2]^+$ complexes. The stable structure at reaction conditions is calculated to be the case with three $HSO_4(NH_4)$, see SM. Using constrained AIMD we find that two $[Cu^I(NH_3)_2]^+$ complexes can not get close enough to allow for O_2 adsorption in the presence of three $HSO_4(NH_4)$ species in the cage, see S7. Thus, from kinetic and thermodynamic considerations up to three $HSO_4(NH_4)$ could, in principle, form per $[Cu^I(NH_3)_2]^+$ pair. However, it has been measured that the S/Cu ratio rarely exceeds one [20,25], which indicates alternative origins of deactivation.

The analysis in Fig. 6 is based on the assumption of having two $[Cu^I(NH_3)_2]^+$ complexes in the same cage. Thus, the stability of paired $[Cu^I(NH_3)_2]^+$ complexes in the presence of bulky $HSO_4(NH_4)$ is critical. To investigate the stability, we have performed constrained AIMD simulations for three scenarios with different numbers of $HSO_4(NH_4)$. The simulations are shown in Fig. 7 (more information can be found in SM). The simulations are performed with two $[Cu^I(NH_3)_2]^+$ complexes, studying the diffusion of one of the complexes through an eight-membered ring to a neighboring cage. The energies are reported with respect to the situation with the complexes in two different cages. For the case without any $HSO_4(NH_4)$ (only complexes), a barrier of 0.3 eV is calculated, which is in agreement with a previous report using CI-NEB [15]. The situation with two complexes in the same cage is slightly preferred. The presence of one $HSO_4(NH_4)$ inside the cage, further stabilizes the paring of $[Cu^I(NH_3)_2]^+$. The situation is qualitatively changed in the presence of two $HSO_4(NH_4)$. The free energy in presence of two $HSO_4(NH_4)$ is lower for the case with complexes in separate cages. Moreover, the barrier for diffusion is lowered to 0.1 eV. The simulations suggest that sulfur deactivation originates from a low probability of having paired $[Cu^I(NH_3)_2]^+$ complexes as the presence of multiple $HSO_4(NH_4)$ favours the separation of the $[Cu^I(NH_3)_2]^+$ complexes.

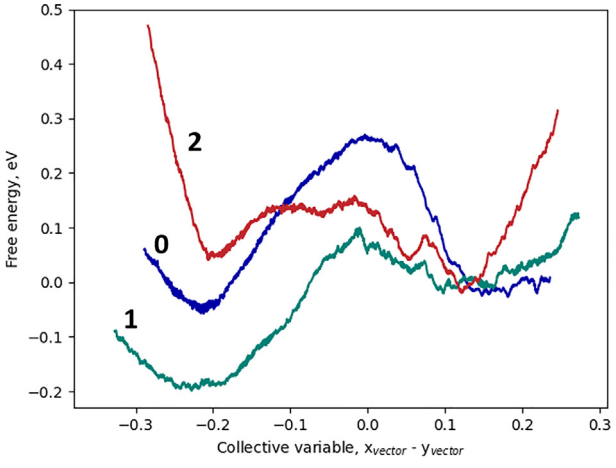

Fig. 7. AIMD simulation of the free energy profiles for diffusion of a $[Cu^I(NH_3)_2]^+$ complex through an eight-membered ring in the presence of a second $[Cu^I(NH_3)_2]^+$ and different numbers of $HSO_4(NH_4)$ species. The simulations are done with zero (blue), one (green) or two (red) $HSO_4(NH_4)$ located in one of cages. (For interpretation of the references to colour in this figure legend, the reader is referred to the web version of this article.)

4. Discussion

The main results of the presented calculations are that i) $HSO_4(NH_4)$ is the preferred species from the reaction of SO_2 with the $[Cu^{II}_2(NH_3)_4O_2]^{2+}$ peroxo complex and that ii) the presence of multiple $HSO_4(NH_4)$ species hinder O_2 adsorption by effectively separating the two $[Cu^I(NH_3)_2]^+$ complexes. The calculations suggest that the low temperature deactivation of the NH_3-SCR reaction by SO_2 is of physical origin and reversible as $HSO_4(NH_4)$ decompose at elevated temperatures. Here we discuss our results in relation to experimental observations.

Based on SO_2-TPD, $HSO_4(NH_4)$ and $SO_4(NH_4)_2$ species are suggested to decompose at 420 °C [19,21,23,28], which imply that catalysts deactivated by formation of $HSO_4(NH_4)$ can be regenerated by thermal treatment. The lowering of the apparent activation energy measured for reversible deactivation [25] could, thus, be explained by diffusion limitations of the $[Cu^I(NH_3)_2]^+$ complexes. The irreversible deactivation is instead linked to sulfur adsorption on Cu sites, which leads to chemical poisoning. The detailed mechanisms for the irreversible deactivation and the interplay between reversible and irreversible deactivation are open questions for future studies.

Molokova et al. [28] recently investigated SO_2 adsorption on different Cu-species using X-ray absorption spectroscopy. It was concluded that the reaction between SO_2 and $[Cu^{II}_2(NH_3)_4O_2]^{2+}$ contributes significantly to the accumulation of sulfur in Cu-CHA. In addition, it was suggested that sulfur in SO_2 is bonded to copper via an oxygen atom and not directly to the copper atom. The experimental observations concerning the interaction of SO_2 with $[Cu^I(NH_3)_2]^+$ and $[Cu^{II}_2(NH_3)_4O_2]^{2+}$ are in line with our DFT calculations.

Temperature programmed desorption (TPD) experiments are commonly used to distinguish between different sulfur species formed during SO_2 exposure to Cu-CHA. Three peaks measuring the release of SO_2 is observed at 420, 540 and 720 °C. Release of SO_2 at 420 °C is typically assigned to SO_2 stored as $HSO_4(NH_4)$ or $SO_4(NH_4)_2$[19,21,23,28]. The TPD trace from copper-free H-CHA impregnated with $SO_4(NH_4)_2$ has a low-temperature peak at about 380 °C,[28] thus, 40 °C lower than in Cu-CHA. The stabilization of ammonium(bi) sulfate species by Cu is consistent with our AIMD simulations. In the AIMD simulations, we find that the oxygen ions in $HSO_4(NH_4)$ are coordinating to the copper ions, which suggests an attractive electrostatic interaction. Another sign of the

stabilization is that if only one $HSO_4(NH_4)$ is present in the CHA cage, we find that the paring of the $[Cu^I(NH_3)_2]^+$ complexes is stabilized by 0.15 eV as compared to the case without $HSO_4(NH_4)$, see Fig. 7.

The peaks at 540 and 720 °C are commonly attributed to sulfur-containing species bonded directly to either copper or aluminum [19,21]. These TPD peaks are at temperatures where copper is not solvated by ammonia but, instead, bonded directly to the framework, and could possibly be related to the irreversible deactivation. One speculation [19,26] is that sulfur species originating from ammonia bisulfate decomposition could bind directly to Cu or Al, forming $CuSO_x$ or $AlSO_x$ species. Such mechanisms would lead to chemical poisoning and require further exploration.

One important finding is that the presence of $HSO_4(NH_4)$ hinder O_2 adsorption in Cu-CHA. The structure of the zeolite has been measured to affect the SO_2-induced deactivation [56,24]. Recently, the poisoning with SO_2 and SO_3 of Cu-CHA was compared to poisoning of Cu-BEA [24]. It was observed that the deactivation of Cu-CHA was more severe than that of Cu-BEA even if Cu-CHA accumulated only 10 % of the sulfur accumulated in Cu-BEA. The difference was suggested to be related to the differences in cages sizes. The observation is consistent with our results. In Fig. 7, the AIMD simulations show that the pairing is hindered in the presence of more than one $HSO_4(NH_4)$. Larger cages and ring sizes could be expected to reduce the repulsion between species. Moreover, the larger ring size in Cu-BEA, could decrease the diffusion barriers of $HSO_4(NH_4)$, resulting in more evenly distributed $HSO_4(NH_4)$ species.

Our results suggest that the reversible SO_2 deactivation of Cu-CHA originates from a low probability of having paired $[Cu^I(NH_3)_2]^+$ complexes, which is required for O_2 adsorption. The mobility and structural flexibility of the active site is important for the catalytic activity of Cu-CHA. The diffusion of key intermediates have been studied here and elsewhere [16] with ab initio molecular dynamics, which is computationally heavy and restricted to short simulation times and relatively small model systems. More complete exploration of how diffusion and paring of $[Cu^I(NH_3)_2]^+$ complexes is affected by $HSO_4(NH_4)$ would require development of efficient force fields, which is a direction for future studies.

5. Conclusion

We have used density functional theory (DFT) calculation to investigate low temperature SO_2 poisoning of Cu-CHA during NH_3-SCR. SO_2 is found to react with the $[Cu^{II}_2(NH_3)_4O_2]^{2+}$ peroxo complex, which is a critical intermediate. The reaction is exothermic with low barriers, forming N_2, H_2O and H_2SO_4. H_2SO_4 undergoes an acid-base reaction in the presence of NH_3 forming $SO_4(NH_4)_2$ and $HSO_4(NH_4)$. $HSO_4(NH_4)$ is found to be the thermodynamically stable species during typical reaction conditions. The inter-cage diffusion barriers for $HSO_4(NH_4)$ are calcuated to be appreciable, which could result in accumulation of $HSO_4(NH_4)$ in the zeolite cages.

The paring of two $[Cu^I(NH_3)_2]^+$ complexes is required for O_2 activation in the low temperature NH_3-SCR reaction cycle. O_2 adsorption is a key step for the subsequential adsorption of NO and formation of NO^+, which can couple to NH_3. Here we find that the presence of $HSO_4(NH_4)$ species has a large effect on the probability for having two $[Cu^I(NH_3)_2]^+$ in the same cage. Presence of one $HSO_4(NH_4)$ species, yields a stabilization of the paired $[Cu^I(NH_3)_2]^+$ complexes, whereas the presence of two $HSO_4(NH_4)$ species destabilize the situation with two $[Cu^I(NH_3)_2]^+$ complexes in the same cage.

Our results suggest that the SO_2 poisoning at low temperature is of physical origin where the sulfate species hinders the diffusion of the $[Cu^I(NH_3)_2]^+$ complex and possibly the reactants. The studied poisoning is reversible as $HSO_4(NH_4)$ decomposes at elevated temperatures. Our findings provide a link between experiments of SO_2 poisoning and atomic scale mechanisms.

Declaration of Competing Interest

The authors declare that they have no known competing financial interests or personal relationships that could have appeared to influence the work reported in this paper.

Acknowledgement

We acknowledge support from the European Union's Horizon 2020 research and innovation programme under the Marie Sklodowska-Curie grant agreement No. 955839 (CHASS). Additional support from the Swedish Energy Agency (47110–1) is acknowledged. The calculations have been performed at C3SE (Göteborg) and NSC (Linköping) through a SNIC grant. The Competence Centre for Catalysis (KCK) is hosted by Chalmers University of Technology and financially supported by the Swedish Energy Agency (52689–1) and the member companies Johnson Matthey, Perstorp, Powercell, Preem, Scania CV, Umicore and Volvo Group.

Appendix A. Supplementary material

Supplementary data associated with this article can be found, in the online version, at https://doi.org/10.1016/j.jcat.2022.12.023.

References

[1] A. Wang, L. Olsson, The impact of automotive catalysis on the United Nations sustainable development goals, Nature, Catalysis 2 (2019) 566–570, https://doi.org/10.1038/s41929-019-0318-3.
[2] Y. Xin, Q. Li, Z. Zhang, Zeolitic Materials for DeNO$_x$ Selective Catalytic Reduction, ChemCatChem 10 (2018) 29–41, https://doi.org/10.1002/cctc.201700854.
[3] J.H. Kwak, R.G. Tonkyn, D.H. Kim, J. Szanyi, C.H.F. Peden, Excellent activity and selectivity of Cu-SSZ-13 in the selective catalytic reduction of NO$_x$ with NH_3, J. Catal. 275 (2010) 187–190, https://doi.org/10.1016/j.jcat.2010.07.031.
[4] D.W. Fickel, E. D'Addio, J.A. Lauterbach, R.F. Lobo, The ammonia selective catalytic reduction activity of copper-exchanged small-pore zeolites, Appl. Catal. B: Environmental 102 (2011) 441–448, https://doi.org/10.1016/j.apcatb.2010.12.022.
[5] S.J. Schmieg, S.H. Oh, C.H. Kim, D.B. Brown, J.H. Lee, C.H.F. Peden, D.H. Kim, Thermal durability of Cu-CHA NH_3-SCR catalysts for diesel NO$_x$ reduction, Catal. Today 184 (2012) 252–261, https://doi.org/10.1016/j.cattod.2011.10.034.
[6] F. Gramigni, N.D. Nasello, N. Usberti, U. Iacobone, T. Selleri, W. Hu, S. Liu, X. Gao, I. Nova, E. Tronconi, Transient Kinetic Analysis of Low-Temperature NH_3-SCR over Cu-CHA Catalysts Reveals a Quadratic Dependence of Cu Reduction Rates on Cu^{II}, ACS Catal. 11 (2021) 4821–4831, https://doi.org/10.1021/acscatal.0c05362.
[7] C. Paolucci, I. Khurana, A.A. Parekh, S. Li, A.J. Shih, H. Li, J.R.D. Iorio, J.D. Albarracin-Caballero, A. Yezerets, J.T. Miller, W.N. Delgass, F.H. Ribeiro, W.F. Schneider, R. Gounder, Dynamic multinuclear sites formed by mobilized copper ions in NO$_x$ selective catalytic reduction, Science 357 (2017) 898–903, https://doi.org/10.1126/science.aan5630.
[8] F. Gao, D. Mei, Y. Wang, J. Szanyi, C.H.F. Peden, Selective Catalytic Reduction over Cu/SSZ-13: Linking Homo- and Heterogeneous Catalysis, J. Am. Chem. Soc. 139 (2017) 4935–4942, https://doi.org/10.1021/jacs.7b01128.

[9] J.H. Kwak, H. Zhu, J.H. Lee, C.H.F. Peden, J. Szanyi, Two different cationic positions in Cu-SSZ-13?, Chem Commun. 48 (2012) 4758–4760, https://doi.org/10.1039/C2CC31184D.

[10] C. Paolucci, A.A. Parekh, I. Khurana, J.R. Di Iorio, H. Li, J.D. Albarracin Caballero, A.J. Shih, T. Anggara, W.N. Delgass, J.T. Miller, F.H. Ribeiro, R. Gounder, W.F. Schneider, Catalysis in a Cage: Condition-Dependent Speciation and Dynamics of Exchanged Cu Cations in SSZ-13 Zeolites, J. Am. Chem. Soc. 138 (2016) 6028–6048, https://doi.org/10.1021/jacs.6b02651.

[11] A. Marberger, A.W. Petrov, P. Steiger, M. Elsener, O. Kröcher, M. Nachtegaal, D. Ferri, Time-resolved copper speciation during selective catalytic reduction of NO on Cu-SSZ-13, Nature Catal. 1 (2018) 221–227, https://doi.org/10.1038/s41929-018-0032-6.

[12] K.A. Lomachenko, E. Borfecchia, C. Negri, G. Berlier, C. Lamberti, P. Beato, H. Falsig, S. Bordiga, The Cu-CHA deNO$_x$ Catalyst in Action: Temperature-Dependent NH$_3$-Assisted Selective Catalytic Reduction Monitored by Operando XAS and XES, J. Am. Chem. Soc. 138 (2016) 12025–12028, https://doi.org/10.1021/jacs.6b06809.

[13] L. Chen, H. Falsig, T.V.W. Janssens, H. Grönbeck, Activation of Oxygen on (NH$_3$–Cu–NH$_3$)$^+$ in NH$_3$-SCR over Cu-CHA, J. Catal. 358 (2018) 179–186, https://doi.org/10.1016/j.jcat.2017.12.009.

[14] F. Giordanino, E. Borfecchia, K.A. Lomachenko, A. Lazzarini, G. Agostini, E. Gallo, A.V. Soldatov, P. Beato, S. Bordiga, C. Lamberti, Interaction of NH$_3$ with Cu-SSZ-13 Catalyst: A Complementary FTIR, XANES, and XES Study, J. Phys. Chem. Lett. 5 (2014) 1552–1559, https://doi.org/10.1021/jz500241m.

[15] L. Chen, J. Jansson, M. Skoglundh, H. Grönbeck, Mechanism for Solid-State Ion Exchange of Cu$^+$ into Zeolites, J. Phys. Chem. C 120 (2016) 29182–29189, https://doi.org/10.1021/acs.jpcc.6b09553.

[16] R. Millan, P. Cnudde, V. van Speybroeck, M. Boronat, Mobility and Reactivity of Cu$^+$ Species in Cu-CHA Catalysts under NH$_3$-SCR-NO$_x$ Reaction Conditions: Insights from AIMD Simulations, JACS Au 1 (2021) 1778–1787, https://doi.org/10.1021/jacsau.1c00337.

[17] L. Chen, T.V.W. Janssens, P.N.R. Vennestrøm, J. Jansson, M. Skoglundh, H. Grönbeck, A Complete Multisite Reaction Mechanism for Low-Temperature NH$_3$-SCR over Cu-CHA, ACS Catal. 10 (2020) 5646–5656, https://doi.org/10.1021/acscatal.0c00440.

[18] Y. Feng, X. Wang, T.V.W. Janssens, P.N.R. Vennestrøm, J. Jansson, M. Skoglundh, H. Grönbeck, First-Principles Microkinetic Model for Low-Temperature NH$_3$-Assisted Selective Catalytic Reduction of NO over Cu-CHA, ACS Catal. (2021) 14395–14407. doi:10.1021/acscatal.1c03973.

[19] K. Wijayanti, K. Xie, A. Kumar, K. Kamasamudram, L. Olsson, Effect of gas compositions on SO$_2$ poisoning over Cu/SSZ-13 used for NH$_3$-SCR, Appl. Catal. B: Environmental 219 (2017) 142–154, https://doi.org/10.1016/j.apcatb.2017.07.017.

[20] P.S. Hammershøi, A.D. Jensen, T.V.W. Janssens, Impact of SO$_2$-poisoning over the lifetime of a Cu-CHA catalyst for NH$_3$-SCR, Appl. Catal. B: Environmental 238 (2018) 104–110, https://doi.org/10.1016/j.apcatb.2018.06.039.

[21] Y. Xi, N. Ottinger, C. Su, Z.G. Liu, Sulfur Poisoning of a Cu-SSZ-13 SCR Catalyst under Simulated Diesel Engine Operating Conditions, SAE 3 (2021) 2690–2694, https://doi.org/10.4271/2021-01-0576.

[22] A.J. Shih, I. Khurana, H. Li, J. González, A. Kumar, C. Paolucci, T.M. Lardinois, C.B. Jones, J.D. Albarracin Caballero, K. Kamasamudram, A. Yezerets, W.N. Delgass, J.T. Miller, A.L. Villa, W.F. Schneider, R. Gounder, F.H. Ribeiro, Spectroscopic and kinetic responses of Cu-SSZ-13 to SO$_2$ exposure and implications for NO$_x$ selective catalytic reduction, Appl. Catal. A: General 574 (2019) 122–131, https://doi.org/10.1016/j.apcata.2019.01.024.

[23] Y. Jangjou, Q. Do, Y. Gu, L.-G. Lim, H. Sun, D. Wang, A. Kumar, J. Li, L.C. Grabow, W.S. Epling, Nature of Cu Active Centers in Cu-SSZ-13 and Their Responses to SO$_2$ Exposure, ACS Catal. 8 (2018) 1325–1337, https://doi.org/10.1021/acscatal.7b03095.

[24] X. Auvray, M. Arvanitidou, Å. Högström, J. Jansson, S. Fouladvand, L. Olsson, Comparative Study of SO$_2$ and SO$_2$/SO$_3$ Poisoning and Regeneration of Cu/BEA and Cu/SSZ-13 for NH3 SCR, Emiss. Control, Sci. Technol. 7 (2021) 232–246, https://doi.org/10.1007/s40825-021-00203-4.

[25] P.S. Hammershøi, Y. Jangjou, W.S. Epling, A.D. Jensen, T.V.W. Janssens, Reversible and irreversible deactivation of Cu-CHA NH$_3$-SCR catalysts by SO$_2$ and SO$_3$, Appl. Catal. B: Environmental 226 (2018) 38–45, https://doi.org/10.1016/j.apcatb.2017.12.018.

[26] V. Mesilov, S. Dahlin, S.L. Bergman, S. Xi, J. Han, L. Olsson, L.J. Pettersson, S.L. Bernasek, Regeneration of sulfur-poisoned Cu-SSZ-13 catalysts: Copper speciation and catalytic performance evaluation, Appl. Catal. B: Environmental 299 (2021) 120626, https://doi.org/10.1016/j.apcatb.2021.120626.

[27] V.V. Mesilov, S.L. Bergman, S. Dahlin, Y. Xiao, S. Xi, M. Zhirui, L. Xu, W. Chen, L.J. Pettersson, S.L. Bernasek, Differences in oxidation-reduction kinetics and mobility of Cu species in fresh and SO$_2$-poisoned Cu-SSZ-13 catalysts, Appl. Catal. B: Environmental 284 (2021) 119756, https://doi.org/10.1016/j.apcatb.2020.119756.

[28] A.Y. Molokova, E. Borfecchia, A. Martini, I.A. Pankin, C. Atzori, O. Mathon, S. Bordiga, F. Wen, P.N.R. Vennestrøm, G. Berlier, T.V.W. Janssens, K.A. Lomachenko, SO$_2$ Poisoning of Cu-CHA deNO$_x$ Catalyst: The Most Vulnerable Cu Species Identified by X-ray Absorption Spectroscopy, JACS Au 2 (2022) 787–792, https://doi.org/10.1021/jacsau.2c00053.

[29] W. Hu, T. Selleri, F. Gramigni, E. Fenes, K.R. Rout, S. Liu, I. Nova, D. Chen, X. Gao, E. Tronconi, On the Redox Mechanism of Low-Temperature NH$_3$-SCR over Cu-CHA: A Combined Experimental and Theoretical Study of the Reduction Half Cycle, Angew. Chem. Int. Ed. 60 (2021) 7197–7204, https://doi.org/10.1002/anie.202014926.

[30] T.J. Goncalves, P.N. Plessow, F. Studt, Theoretical Study on the NO$_x$ Selective Catalytic Reduction on Single-Cu Sites and Brønsted Acid Sites in Cu-SSZ-13, J. Phys. Chem. C 125 (2021) 12594–12602, https://doi.org/10.1021/acs.jpcc.1c01066.

[31] V. Mesilov, Y. Xiao, S. Dahlin, S.L. Bergman, L.J. Pettersson, S.L. Bernasek, First-Principles Calculations of Condition-Dependent Cu/Fe Speciation in Sulfur-Poisoned Cu- and Fe-SSZ-13 Catalysts, J. Phys. Chem. C 125 (2021) 4632–4645, https://doi.org/10.1021/acs.jpcc.1c01016.

[32] P.S. Hammershøi, P.N.R. Vennestrøm, H. Falsig, A.D. Jensen, T.V.W. Janssens, Importance of the Cu oxidation state for the SO$_2$-poisoning of a Cu-SAPO-34 catalyst in the NH$_3$-SCR reaction, Appl. Catal. B: Environmental 236 (2018) 377–383, https://doi.org/10.1016/j.apcatb.2018.05.038.

[33] G. Kresse, J. Furthmüller, Efficient iterative schemes for ab initio total-energy calculations using a plane-wave basis set, Phys. Rev. B 54 (1996) 11169–11186, https://doi.org/10.1103/PhysRevB.54.11169.

[34] G. Kresse, J. Hafner, Ab initio molecular-dynamics simulation of the liquid-metal–amorphous-semiconductor transition in germanium, Phys. Rev. B 49 (1994) 14251–14269, https://doi.org/10.1103/PhysRevB.49.14251.

[35] J.P. Perdew, K. Burke, M. Ernzerhof, Generalized Gradient Approximation Made Simple, Phys. Rev. Lett. 77 (1996) 3865–3868, https://doi.org/10.1103/PhysRevLett.77.3865.

[36] S. Grimme, J. Antony, S. Ehrlich, H. Krieg, A consistent and accurate ab initio parametrization of density functional dispersion correction (DFT-D) for the 94 elements H-Pu, J. Chem. Phys. 132 (2010) 154104, https://doi.org/10.1063/1.3382344.

[37] S.L. Dudarev, G.A. Botton, S.Y. Savrasov, C.J. Humphreys, A.P. Sutton, Electron-energy-loss spectra and the structural stability of nickel oxide: An LSDA+U study, Phys. Rev. B 57 (1998) 1505–1509, https://doi.org/10.1103/PhysRevB.57.1505.

[38] L. Chen, T.V.W. Janssens, H. Grönbeck, A comparative test of different density functionals for calculations of NH$_3$ -SCR over Cu-Chabazite, Phys. Chem. Chem. Phys. 21 (2019) 10923–10930, https://doi.org/10.1039/C9CP01576K.

[39] T. Anggara, C. Paolucci, W.F. Schneider, Periodic DFT Characterization of NOx Adsorption in Cu-Exchanged SSZ-13 Zeolite Catalysts, J. Phys. Chem. C 120 (2016) 27934–27943, https://doi.org/10.1021/acs.jpcc.6b07972.

[40] P.E. Blöchl, Projector augmented-wave method, Phys. Rev. B 50 (1994) 17953–17979, https://doi.org/10.1103/PhysRevB.50.17953.

[41] G. Kresse, D. Joubert, From ultrasoft pseudopotentials to the projector augmented-wave method, Phys. Rev. B 59 (1999) 1758–1775, https://doi.org/10.1103/PhysRevB.59.1758.

[42] G. Mills, H. Jónsson, G.K. Schenter, Reversible work transition state theory: Application to dissociative adsorption of hydrogen, Surf. Sci. 324 (1995) 305–337, https://doi.org/10.1016/0039-6028(94)00731-4.

[43] G. Henkelman, H. Jónsson, Improved tangent estimate in the nudged elastic band method for finding minimum energy paths and saddle points, J. Chem. Phys. 113 (2000) 9978–9985, https://doi.org/10.1063/1.1323224.

[44] S. Nosé, A unified formulation of the constant temperature molecular dynamics methods, J. Chem. Phys. 81 (1984) 511–519, https://doi.org/10.1063/1.447334.

[45] W.G. Hoover, Canonical dynamics: Equilibrium phase-space distributions, Phys. Rev. A 31 (1985) 1695–1697, https://doi.org/10.1103/PhysRevA.31.1695.

[46] E.A. Carter, G. Ciccotti, J.T. Hynes, R. Kapral, Constrained reaction coordinate dynamics for the simulation of rare events, Chem. Phys. Lett. 156 (1989) 472–477, https://doi.org/10.1016/S0009-2614(89)87314-2.

[47] W. Tang, E. Sanville, G. Henkelman, A grid-based Bader analysis algorithm without lattice bias, J. Phys.: Condensed Matter 21 (2009) 084204, https://doi.org/10.1088/0953-8984/21/8/084204.

[48] M. Yu, D.R. Trinkle, Accurate and efficient algorithm for Bader charge integration, J. Chem. Phys. 134 (2011) 064111, https://doi.org/10.1063/1.3553716.

[49] F. Göltl, R.E. Bulo, J. Hafner, P. Sautet, What Makes Copper-Exchanged SSZ-13 Zeolite Efficient at Cleaning Car Exhaust Gases?, J Phys. Chem. Lett. 4 (2013) 2244–2249, https://doi.org/10.1021/jz400817c.

[50] L. Chen, H. Falsig, T.V.W. Janssens, J. Jansson, M. Skoglundh, H. Grönbeck, Effect of Al-distribution on oxygen activation over Cu–CHA, Catal, Sci. Technol. 8 (2018) 2131–2136, https://doi.org/10.1039/C8CY00083B.

[51] M. Chase, NIST-JANAF Thermochemical Tables, 4th Edition,., American Institute of Physics, 1998, p. -1.

[52] M. Jørgensen, L. Chen, H. Grönbeck, Monte Carlo Potential Energy Sampling for Molecular Entropy in Zeolites, J. Phys. Chem. C 122 (2018) 20351–20357, https://doi.org/10.1021/acs.jpcc.8b05382.

[53] C. Negri, T. Selleri, E. Borfecchia, A. Martini, K.A. Lomachenko, T.V.W. Janssens, M. Cutini, S. Bordiga, G. Berlier, Structure and Reactivity of Oxygen-Bridged Diamino Dicopper(II) Complexes in Cu-Ion-Exchanged Chabazite Catalyst for NH$_3$-Mediated Selective Catalytic Reduction, J. Am. Chem. Soc. 142 (2020) 15884–15896, https://doi.org/10.1021/jacs.0c06270.

[54] V. Mesilov, S. Dahlin, S.L. Bergman, P.S. Hammershøi, S. Xi, L.J. Pettersson, S.L. Bernasek, Insights into sulfur poisoning and regeneration of Cu-SSZ-13 catalysts: In situ Cu and S K-edge XAS studies, Catal, Sci. Technol. 11 (2021) 5619–5632, https://doi.org/10.1039/D1CY00975C.
[55] X. Yong, H. Chen, H. Zhao, M. Wei, Y. Zhao, Y. Li, Insight into SO_2 poisoning and regeneration of one-pot synthesized Cu-SSZ-13 catalyst for selective reduction of NO_x by NH_3, Chin. J. Chem. Eng. 46 (2022) 184–193, https://doi.org/10.1016/j.cjche.2021.06.012.
[56] A. Wang, L. Olsson, Insight into the SO_2 poisoning mechanism for NO_x removal by NH_3-SCR over Cu/LTA and Cu/SSZ-13, Chem. Eng. J. 395 (2020) 125048, https://doi.org/10.1016/j.cej.2020.125048.